Proc. Natl. Acad. Sci. USA
Vol. 92, pp. 2121–2125, March 1995
Biophysics

Voltage-dependent gating of an asymmetric gramicidin channel

(lipid bilayers/hexafluorovaline/conformational changes)

SHIGETOSHI OIKI†‡, ROGER E. KOEPPE II§, AND OLAF S. ANDERSEN†

†Department of Physiology and Biophysics, Cornell University Medical College, New York, NY 10021; ‡Department of Cellular and Molecular Physiology, National Institute for Physiological Sciences, Okazaki 444, Japan; and §Department of Chemistry and Biochemistry, University of Arkansas, Fayetteville, AR 72701

Communicated by Bertil Hille, University of Washington, Seattle, WA, November 17, 1994 (received for review August 10, 1994)

ABSTRACT **In an effort to understand the molecular mechanisms of voltage activation of ion channels, we have chosen a system of known structure and examined the properties of heterodimeric channels formed between [Val^1]gramicidin A ([Val^1]gA) and [F_6Val^1]gramicidin A ([F_6Val^1]gA). Gramicidin channels are usually not voltage-dependent; but the introduction of a single symmetry-breaking dipolar F_6Val^1 residue into a ([Val^1]gA)$_2$ dimer to form the [F_6Val^1]gA/[Val^1]gA heterodimer induces voltage-dependent transitions between two conducting states: a high-conductance state and a zero conductance (closed) state. The distribution between these states varies as a function of the applied potential but is not dependent on the nature of the permeant ion (H^+ or Cs^+). The permeating ions do not seem to contribute to the apparent gating charge.**

Gramicidin channels are one of only two classes of ion channels for which an atomic resolution structure is available (1, 2), the other being the porins (3). As suggested by Urry (4), gramicidin channels are dimers of $\beta^{6.3}$-helical monomers that are joined by six hydrogen bonds at their formyl-NH termini. Gramicidin channels form by the transmembrane dimerization of two nonconducting monomers (5); a channel appearance/disappearance event, therefore, usually denotes the spontaneous formation and dissociation of the conducting (membrane-spanning) dimer (for reviews, see refs. 6–8).

Taking [Val^1]gramicidin A ([Val^1]gA) as the reference, gramicidin analogues with position 1 substitutions form symmetrical homodimers whose single-channel conductance (g) and average duration (τ) can vary 10-fold. These "mutant" channels are structurally equivalent to homodimeric [Val^1]gA channels because heterodimers (hybrid channels) form freely between the different analogues and [Val^1]gA (9). If we view the [Val^1]gA dimer as the wild-type channel, then heterodimers are singly mutated channels and homodimers are doubly mutated channels. Not surprisingly, hybrid channels usually have properties (g and τ) that are intermediate to those of the parent homodimers (9).

Gramicidins with 4,4,4,4′,4′,4′-hexafluorovaline (F_6Val) at position 1 violate this pattern, because the single-substituted [F_6Val^1]gA/[Val^1]gA channels have a lower g and shorter τ than either symmetrical parent channel (9–11). Hybrid channels form freely between [F_6Val^1]gA and [Val^1]gA, but the heterodimers are destabilized, indicating that there is a strain at the junction between the monomers (9). Further, and in contrast to other heterodimers, [F_6Val^1]gA/[Val^1]gA channels exhibit rapid transitions between at least two current levels (12).

To understand more fully the properties of the heterodimeric channels formed by [F_6Val^1]gA and [Val^1]gA, we have examined these channels in solvent-depleted phospholipid bilayers by using a modified tip-dip method (13). The solvent depletion confers longer average durations on the channels; and the tip-dip approach allows for better signal/noise characteristics and higher current resolution. In this article we characterize the voltage-dependent gating of [F_6Val^1]gA/[Val^1]gA channels when the permeant ion is either Cs^+ or H^+. These two ions were chosen because Cs^+ and H_2O move through gramicidin channels in a single file, whereas H^+ can jump along the chain of H_2O molecules via a proton relay mechanism (14). We conclude that the gating is an intrinsic channel property that is independent of the permeant cation and involves a physical "occlusion" of the pore; this allows us to propose a molecular mechanism for the gating.

MATERIALS AND METHODS

Position 1-substituted gramicidins were synthesized and purified as described (9, 10, 15). F_6Val was purchased from Fairfield Chemicals (Blythwood, SC) as a mixture of D- and L-F_6Val. The enantiomers were not separated because experiments with other analogues ([Val^1]gA and [Phe^1]gA) have suggested that the analogue with the D-enantiomer should be inert (unable to form $\beta^{6.3}$-helical dimers).

Lipid bilayers were formed at the tip of silanized borosilicate glass pipettes from diphytanoylphosphatidylcholine/n-hexadecane (with Cs^+ as the permeant ion) or diphytanoylphosphatidylcholine/squalane (with H^+ as the permeant ion) monolayers spread on the air/electrolyte interface (13). The electrolyte was 1.0 M CsCl or 0.1 M HCl at 25 ± 2°C. Single-channel currents were recorded by using a Dagan 3900 amplifier (Dagan Instruments, Minneapolis), stored on a PCM-VCR (Unitrade/Dagan), filtered by using an 8-pole Bessel filter (Frequency Devices, Haverhill, MA), digitized at 5 times the (−3 dB) filter frequency, and analyzed by using PCLAMP (Axon Instruments, Foster City, CA). Different kinetic models were compared by using Akaike's asymptotic information criterion (16) or the F test (17).

RESULTS

Fig. 1 shows single-channel current traces observed with Cs^+ as the permeant ion for channels formed by [F_6Val^1]gA and [Val^1]gA. When a gramicidin analogue is added alone to the electrolyte solutions, one observes only homodimeric channels, either ([F_6Val^1]gA)$_2$ channels (Fig. 1*A*) or ([Val^1]gA)$_2$ channels (Fig. 1*B*). When both gramicidins are added together (Fig. 1*C*), one observes the two homodimeric channel types and two new channel types with properties that are quite different from those of the homodimeric channels. These channels are heterodimeric [F_6Val^1]gA/[Val^1]gA channels. While the homodimeric channel types have well-defined conducting states of relatively long durations, the new (heterodimeric) channels occur as brief "bursts" of activity with rapid transitions between low- and high-conductance states

The publication costs of this article were defrayed in part by page charge payment. This article must therefore be hereby marked "*advertisement*" in accordance with 18 U.S.C. §1734 solely to indicate this fact.

Abbreviation: gA, gramicidin A.

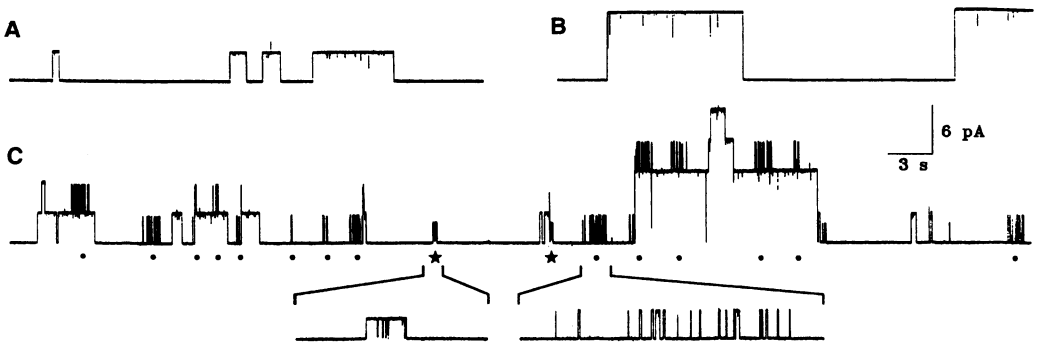

FIG. 1. Gramicidin homodimers and heterodimers: the four channel types observed in the presence of [Val^1]gA and [F_6Val^1]gA. *A* and *B* show traces for homodimeric channels observed in the presence of only a single analogue. (*A*) ([F_6Val^1]gA)$_2$ channels. (*B*) ([Val^1]gA)$_2$ channels. *C* shows channel events observed in the presence of both analogues. In addition to the two homodimeric channels, there are two (bursting) hybrid channel types: high-conductance events (*hh*, denoted by ●) and low-conductance events (*hl*, denoted by ★). An example of each of these events is shown at a 10-fold expanded time scale below the traces in *C*. Conditions: 1.0 M CsCl, 200 mV, and 500 Hz.

(see the expanded trace segments in Fig. 1*C*). These bursts of activity reflect transitions between different conductance states in membrane-spanning dimers (12). There are two heterodimeric channel types that can be distinguished by the different currents in their high-conductance states. The channels with the larger peak currents are denoted *hh*, and the channels with the lower peak currents are denoted *hl*. These two channel types correspond to the two possible orientations of the [F_6Val^1]gA/[Val^1]gA channels with respect to the polarity of the applied potential. When [F_6Val^1]gA and [Val^1]gA are added asymmetrically (one analogue to each side of a bilayer), the *hh* events are seen when the current flow is from [F_6Val^1]gA to [Val^1]gA, and the *hl* events are seen when the current flow is from [Val^1]gA to [F_6Val^1]gA (12). We define the latter polarity as positive. (Both heterodimer orientations are seen in Fig. 1 because both gramicidin analogues are present in both monolayers.)

Both *hl* and *hh* events occur as bursts with rapid transitions between two well-defined current levels, high (**H**) and low (**L**), where the current through the **L** state is indistinguishable from zero (see also Fig. 4). To verify that these bursts result from conductance transitions in membrane-spanning dimers (see ref. 12), the **H**-state duration and interval distributions were examined (Fig. 2). For the *hl* events, the duration distribution of the **H** state can be described by the sum of two exponential distributions (Fig. 2*A1*), which indicates the existence of (at least) two high-conductance events (**H** and **H***). (There was no significant improvement in the fit when the results were fitted by the sum of three exponential distributions.) The corresponding distribution of **L**-state durations and interburst in-

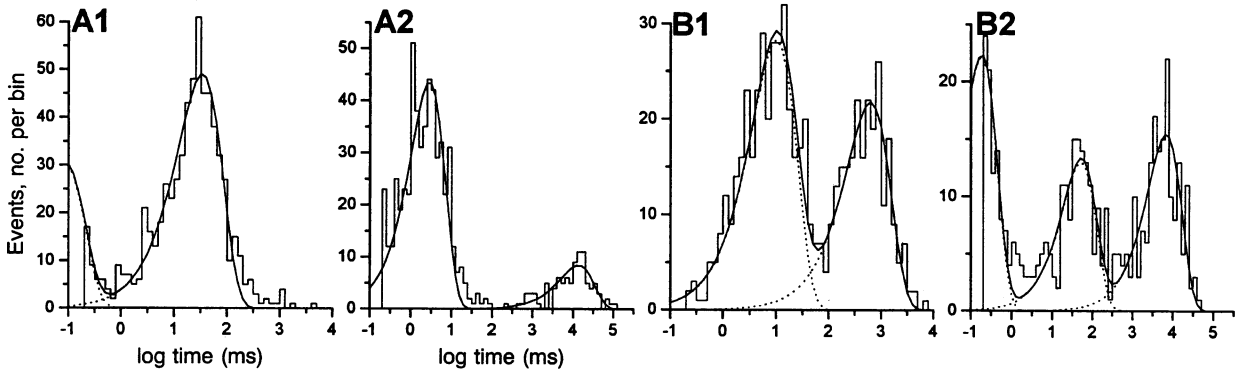

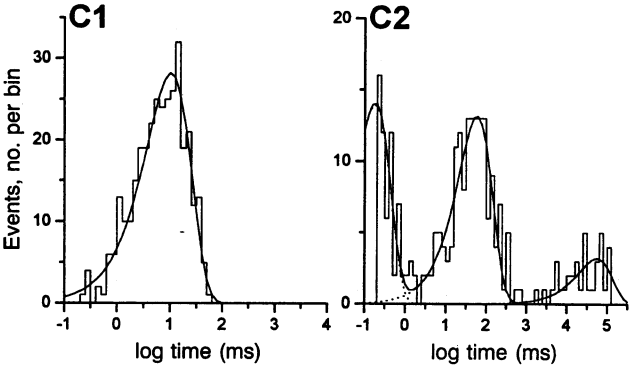

FIG. 2. Duration and interval distributions of [F_6Val^1]gA/[Val^1]gA channels. (*A1*) Duration distribution for *hl* events. The solid curve is the best fit obtained with the sum of two exponential distributions; the interrupted curves are the underlying distributions. The time constants and relative fractions of events are: 0.08 ms and 0.38; 33 ms and 0.62. (*A2*) Corresponding interval distribution. The solid curve is the best fit obtained with the sum of two exponential distributions; the dotted curves are the underlying distributions. The time constants and relative fractions of events are: 2.9 ms and 0.84; 13,600 ms and 0.16. (*B1*) Duration distribution for *hh* events and ([F_6Val^1]gA)$_2$ channels. The solid curve is the best fit obtained with the sum of two exponential distributions; the interrupted curves are the underlying distributions. The time constants and relative fractions of events are: 10 ms and 0.57; and 630 ms and 0.43. The long-lived events are ([F_6Val^1]gA)$_2$ channels. (*B2*) Corresponding interval distribution. The solid curve is the best fit obtained with the sum of three exponential distributions; the dotted curves are the underlying distributions. The time constants and relative fractions of events are: 0.18 ms and 0.44; 52 ms and 0.26; and 6700 ms and 0.30. (*C1*) Duration distribution for *hh* {and ([F_6Val^1]gA)$_2$ events with durations <60 ms}. The solid curve is the best fit obtained with a single exponential distribution. The time constant is 10 ms. (*C2*) Corresponding interval distribution. The solid curve is the best fit obtained with the sum of three exponential distributions; the dotted curves are the underlying distributions. The time constants and relative fractions of events are: 0.18 ms and 0.46; 59 ms and 0.43; and 55,000 ms and 0.11. Results are based on 25-min recording on a single bilayer. Conditions: 1.0 M CsCl, 150 mV, filtered at 4 kHz, and digitized at 20 kHz. The analysis was done by using a 2-kHz digital filter.

tervals (Fig. 2*A2*) can be described by the sum of two exponential distributions (with no significant improvement in the fit when a third component was included). The long-lived population (average duration, 13.6 s) consists of interburst intervals; the short-lived population is intraburst intervals.

For the *hh* events, the **H**-state current is indistinguishable from the current through homodimeric $([F_6Val^1]gA)_2$ channels (12). For the initial analysis of the *hh* events, therefore, the $([F_6Val^1]gA)_2$ channels were included in the analysis; the results are shown in Fig. 2 *B1* and *B2*. The duration distribution is well described by the sum of two exponential distributions (Fig. 2*B1*), where the longer-lived population is $([F_6Val^1]gA)_2$ channels. The corresponding interval distribution can be described by the sum of three exponential distributions (Fig. 2*B2*), where the most long-lived population is interburst intervals. When the analysis is restricted to the *hh* events only, the **H**-state duration distribution can be described by a single exponential distribution (Fig. 2*C1*), while the interval distribution again can be described only by the sum of three exponential distributions (Fig. 2*C2*). Again, the most long-lived population is interburst intervals. The two shorter-lived populations are intraburst intervals, which indicates the existence of (at least) two different low-conductance states (**L** and **L***).

Similar bursting channel activity is not observed with $([Val^1]gA)_2$ or $([F_6Val^1]gA)_2$ channels. We conclude that a burst of *hh* and *hl* activity denotes the formation of a $[F_6Val^1]gA/[Val^1]gA$ channel, which can undergo rapid transitions between (at least) two different conductance states. **H** $\rightleftharpoons$ **L** conductance transitions thus result from conformational changes in intact $\beta^{6.3}$-helical heterodimers. (It is not clear, however, whether the heterodimers always are stabilized by six hydrogen bonds.)

To show more clearly the polarity-dependent heterodimer behavior and the transitions between the **H** and **L** conductance levels, $[F_6Val^1]gA/[Val^1]gA$ channels are shown at a 40-fold expanded time scale in Fig. 3. Fig. 3*A* shows results with Cs^+ as the permeating ion; Fig. 3*B* shows similar results with H^+. For either ion, the $[F_6Val^1]gA/[Val^1]gA$ channels show voltage-dependent gating behavior: the channels tend to reside in the **H** state at positive potentials and in the **L** state at negative potentials. The **L** state has a near-zero conductance at all potentials, irrespective of the identity of the permeant ion.

The very low H^+ conductance of the **L** state of $[F_6Val^1]gA/[Val^1]gA$ channels suggests that the low conductance is due to a severe steric blockage of the pore that prevents H^+ permeation via a proton relay mechanism, which in turn suggests that H_2O cannot pass the block (see ref. 18). We conclude that the gating events result from an alteration in the channel (peptide backbone) structure.

When H^+ is the permeant ion, there are readily discernible brief transitions from the **L** state to some finite current level (Fig. 3*B*). These events are illustrated in more detail in Fig. 4. Fig. 4*A* shows a $[F_6Val^1]gA/[Val^1]gA$ burst with many such transitions and extended segments of the current through the bare bilayer before and after the burst. The expanded record in the lower part of the figure shows the "activity" that occurs in the **L** state and is not present in the baseline current either before or after the burst (upper trace). We assign the duration of a burst to be from the first transition from the zero current level to the **H**-state current level to the last transition (in the burst) back to the zero current level. Fig. 4*B* shows the current level histogram for this event and for the bare bilayer (just before the burst). The current through the (quiescent part of the) **L** state is indistinguishable from the current through the bilayer.

The voltage-dependent **H**/**L** equilibrium was further examined by using current level histograms (Fig. 4*B*) to determine the probability of being in the **H** state (pH) as a function of V: pH is a sigmoid function V and independent of whether Cs^+ or H^+ is the permeant ion (Fig. 5*A*). The shape of the $p\mathrm{H}(V)$ relation is similar to that of conventional (Hodgkin–Huxley) activation curves observed for many different voltage-dependent channel types (19). The results were fitted by models with two, three, and four states, and the quality of the fits were evaluated by using Akaike's asymptotic information criterion (16). The kinetic analysis in Fig. 2 shows the presence of two components in both the **H** and the **L** duration distributions; not surprisingly, the best fit to the results in Fig. 5 was obtained with a four-state model with two high-conductance states (denoted **H** and **H***) and two low-conductance states (denoted **L** and **L***), with **H*** and **L*** being intermediate states. The solid curve in Fig. 5*A* denotes the best fit of the four-state model in Fig. 5*B* to the Cs^+ results by using the 0 mV equilibrium constants and apparent gating valences indicated in Fig. 5*B*.

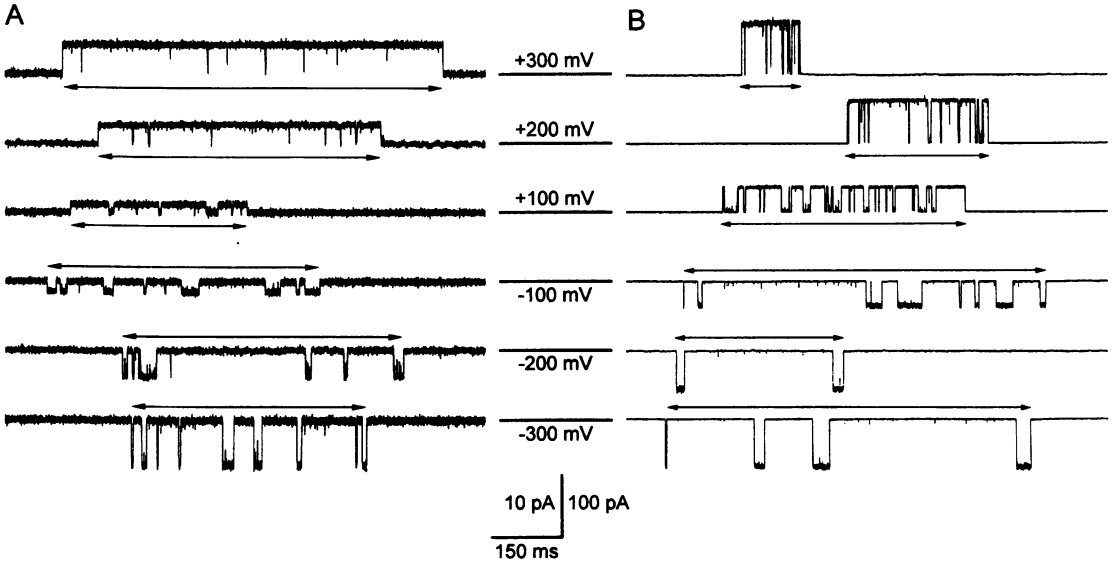

FIG. 3. Cs^+ and H^+ currents through $[F_6Val^1]gA/[Val^1]gA$ channels. (*A*) Cs^+ permeation at different potentials (1.0 M CsCl). (*B*) H^+ permeation at the corresponding potentials (0.1 M HCl). Polarity was as in Fig. 1: upward deflections denote current flow from the $[Val^1]gA$ to the $[F_6Val^1]gA$ half of the channel. The arrow with each trace denotes the dimer duration, which was determined as the time from the first transition to the **H** level to the last transition back to the zero current level; the horizontal lines between the traces denote the bilayer current level.

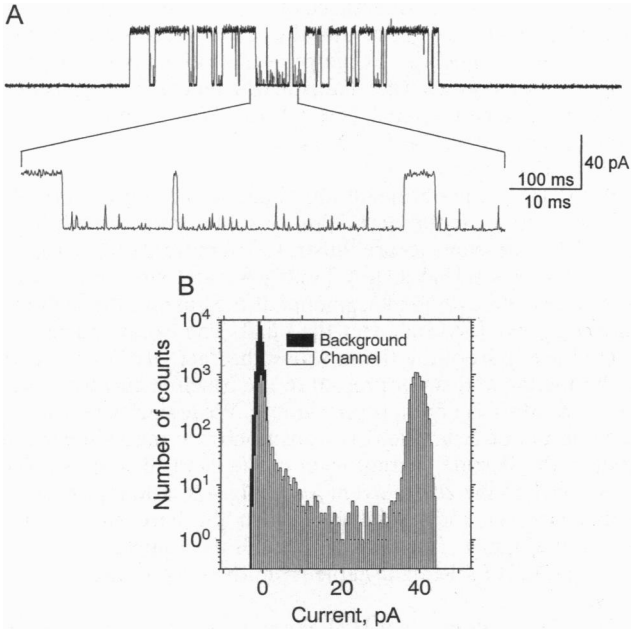

FIG. 4. Further analysis of $[F_6Val^1]gA/[Val^1]gA$ channels with H^+ as the permeating ion. (*A*) Burst of $[F_6Val^1]gA/[Val^1]gA$ channel activity. The upper trace shows the current before, during, and after the burst. Before and after the burst, the current noise is small; during the burst, there is substantial "activity" in the **L** state. The expanded segment shows a stretch of **L**-state activity at an 10-fold expanded time scale. Conditions: 0.1 M HCl, 100 mV, and filtered at 5 kHz. (*B*) Current-level histograms for the background current (solid bars) and for the burst (open bars). The **L**-state current was estimated to be 0.39 pA (after excluding the "shoulder" to the right of the major peak), which is <1% of the **H**-state current and indistinguishable from the background current.

DISCUSSION

We have shown that $[F_6Val^1]gA/[Val^1]gA$ channels display voltage-dependent gating behavior, with transitions between a low-conductance (closed) state and a high-conductance (open) state. The voltage-dependent gating does not depend on the identity of the permeant ion (Fig. 5). The conductance of the **L** state is indistinguishable from zero, even when H^+ is the permeant ion, which indicates that the pore lumen is occluded (at least to the extent that H^+ cannot jump from H_2O to H_2O across the occlusion) and that H_2O cannot move through $[F_6Val^1]gA/[Val^1]gA$ channels in the **L** state. This result also implies that the permeating ions do not contribute to the apparent gating charge. We conclude that the gating is an intrinsic channel property that is uncoupled to ion movement into or through the pore. The $\mathbf{H} \rightleftharpoons \mathbf{L}$ transitions are likely to result from a substantial alteration in channel structure; but the basic $\beta^{6.3}$-helical structure is preserved, as shown by the results in Figs. 2 and 4 and by the finite conductance of the **L** state of $[F_6Val^1]gA/[Gly^1]gA$ heterodimers (11, 12). $[F_6Val^1]gA$-based heterodimers thus form voltage-dependent channels in which the molecular architecture of the gating assembly is known.

The gating occurs in a channel that does not possess fixed charges, which raises questions for voltage-dependent gating in general. In voltage-dependent cation channels, for example, the large-scale voltage dependence is ascribed to the positive charges in the S4 segment (20, 21). The magnitude of the apparent charge movement [≈3 elementary charges per subunit in Shaker potassium channels (22)] could suggest that channel gating involves very substantial conformational changes. The present results, however, show that a considerable voltage dependence can arise in the absence of a frank charge displacement. In addition, the present system serves as a model for conformational transitions in β-sheet-like structures because there exists a high-resolution channel structure (1, 2) that provides hints about the underlying mechanism(s) and constrains the model building. Our results may thus help understand how the putative movement of the S4 segment could be coupled to a channel's closed ⇌ open transitions. We will in the remaining discussion consider the molecular basis for the voltage-dependent $\mathbf{H} \rightleftharpoons \mathbf{L}$ transitions in $[F_6Val^1]gA/[Val^1]gA$ channels.

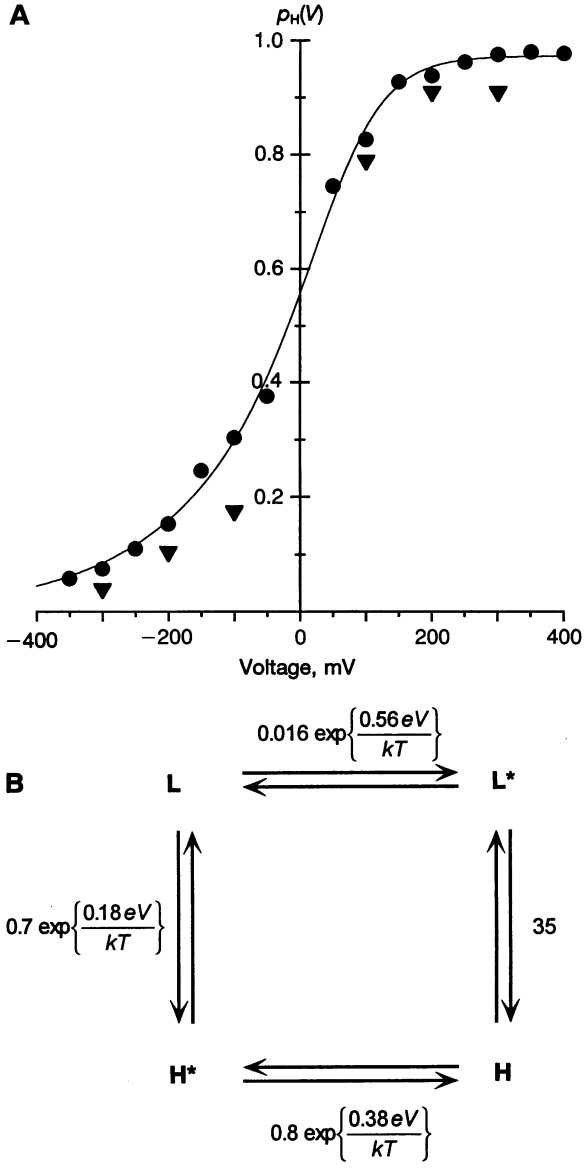

FIG. 5. Voltage-dependent single-channel gating. (*A*) $p_H(V)$ for $[F_6Val^1]gA/[Val^1]gA$ channels with either Cs^+ (●) or H^+ (▼) as the permeant ion. The Cs^+ results were fitted by using the four-state gating model shown in *B*, in which the voltage-dependent equilibrium distribution among the states is described by a Boltzmann expression: $K(0)\cdot\exp\{-zeV/kT\}$, where $K(0)$ is the equilibrium constant at 0 mV and z is the apparent valence. (*B*) The model (with two high-conductance, **H** and **H***, and two low-conductance, **L** and **L***, states) and the 0 mV equilibrium constants and apparent valences.

(*i*) The results should be considered in the perspective of results obtained with other substituted gramicidin channels. When F_6Val [with a dipole moment in the $C_\beta,C_\gamma,C_{\gamma'}$ plane of 1.6 debye (1 debye = 3.338×10^{-30} m·C); see ref. 10] is replaced by the related F_3Val (which also has dipole moment of 1.6 debye in the $C_\beta,C_\gamma,C_{\gamma'}$ plane, albeit along a different axis), the resulting $[F_6Val^1]gA/[Val^1]gA$ heterodimers {or

($[F_3Val^1]gA)_2$ homodimers} do not show similar conductance transitions (10). Similar unexceptional behavior is observed with other dipolar position 1-substituted analogues (10). When Val^1 is replaced by Gly, however, the resulting $[F_6Val^1]gA/[Gly^1]gA$ heterodimers are similar to $[F_6Val^1]gA/[Val^1]gA$ heterodimers, except for a much less pronounced voltage dependence (11, 12). In this series of substitutions, F_6Val^1 is a prerequisite for voltage-dependent gating, but the detailed gating behavior varies as a function of nondipolar substitutions elsewhere in the channel.

(*ii*) Whereas the introduction of a dipolar residue at position 1 can reduce the single-channel current substantially (10), the zero current in the **L** state is too low to result from ion–dipole interactions or inductive electron withdrawal from the carbonyl oxygen in the F_6Val^1 residue (see ref. 23). Moreover, such a mechanism would not account for the presence of two conductance states or why $([F_6Val^1]gA)_2$ channels have a Cs^+ permeability that is higher than that of $([F_3Val^1]gA)_2$ channels (10). The conductance transitions must result from alterations in channel structure.

(*iii*) There are no fixed charges in $[F_6Val^1]gA/[Val^1]gA$ heterodimers, and the gating valences presumably are related to a reorientation of the dipolar F_6Val^1 side chain, possibly in combination with a rearrangement of the peptide backbone. Based on the sign of the gating valences (Fig. 5*B*), it is likely that the **H** state is favored when the negative end of the F_6Val dipole (the two CF_3 groups) is directed away from the $[F_6Val^1]gA$ monomer (i.e., when the χ_1 torsion angle is within the range of $-60°$ to $+60°$). A simple rotation of the F_6Val^1 dipole cannot account for the observed gating behavior, however. By assuming that the applied potential drops linearly over the channel length, the apparent gating valence (z_d) associated with a maximal 180° rotation about the C_α–C_β axis of F_6Val can be approximated as $z_d \approx 2\mu/l$ (where μ is the dipole moment in the C_β,C_γ,$C_{\gamma'}$ plane and l is the channel length): $z_d \approx 0.027$—or only $\approx 5\%$ of the 0.56 needed to account for the voltage dependence of the $\mathbf{L} \rightleftharpoons \mathbf{L^*}$ transition (see Fig. 5). A "free" rotation of the F_6Val^1 side-chain dipole can account for only a small fraction of the apparent gating charge.

The rotation of the side-chain dipole is not "free," however, but is constrained by the rest of channel. In preliminary conformational energy calculations, we find that the rotation of the F_6Val^1 side chain around its C_α–C_β axis is constrained relative to that of Val^1. The main steric conflicts are between the F_6Val side chain and its own backbone, Val^7 in the same monomer, or Ala^5 in the other monomer. The constraints vary with the rotameric state of Val^7. The calculations suggest that short-range interactions stress the backbones of both monomers when the F_6Val dipole is rotated. The movement of the dipole thus can serve as a "trigger" or "gating sensor" for more extensive conformational changes. This type of gating mechanism is likely to be a general feature of ion channels.

We thank Dr. D. B. Sawyer for assistance with developing the tip-dip method. This work was supported by grants from the National Institutes of Health (GM21342 and GM34986) and the Ministry of Education, Science and Culture (Japan).

1. Arseniev, A. S., Lomize, A. L., Barsukov, I. L. & Bystrov, V. F. (1986) *Biol. Membr.* **3,** 1077–1104.
2. Ketchem, R. R., Hu, W. & Cross, T. A. (1993) *Science* **261,** 1457–1460.
3. Weiss, M. S., Abele, U., Weckesser, J., Welte, W., Schiltz, E. & Schulz, G. E. (1991) *Science* **254,** 1627–1630.
4. Urry, D. W. (1971) *Proc. Natl. Acad. Sci. USA* **68,** 672–676.
5. O'Connell, A. M., Koeppe, R. E., II, & Andersen, O. S. (1990) *Science* **250,** 1256–1259.
6. Andersen, O. S. & Koeppe, R. E., II (1992) *Physiol. Rev.* **72,** Suppl., 89–158.
7. Killian, J. A. (1992) *Biochim. Biophys. Acta* **1113,** 391–425.
8. Busath, D. D. (1993) *Annu. Rev. Physiol.* **55,** 473–501.
9. Durkin, J. T., Koeppe, R. E., II, & Andersen, O. S. (1990) *J. Mol. Biol.* **211,** 221–234.
10. Russell, E. W. B., Weiss, L. B., Navetta, F. I., Koeppe, R. E., II, & Andersen, O. S. (1986) *Biophys. J.* **49,** 673–686.
11. Oiki, S., Koeppe, R. E., II, & Andersen, O. S. (1992) *Biophys. J.* **62,** 28–30.
12. Oiki, S., Koeppe, R. E., II, & Andersen, O. S. (1994) *Biophys. J.* **66,** 1823–1832.
13. Sawyer, D. B., Oiki, S. & Andersen, O. S. (1990) *Biophys. J.* **57,** 100 (abstr.).
14. Levitt, D. G., Elias, S. R. & Hautman, J. M. (1978) *Biochim. Biophys. Acta* **512,** 436–451.
15. Weiss, L. B. & Koeppe, R. E., II (1985) *Int. J. Pept. Protein Res.* **26,** 305–310.
16. Akaike, H. (1974) *IEEE Trans. Autom. Control* **AC-19,** 716–723.
17. Ellis, K. J. & Duggleby, R. G. (1978) *Biochem. J.* **171,** 513–517.
18. Stankovic, C. J., Heinemann, S. H. & Schreiber, S. L. (1990) *J. Am. Chem. Soc.* **112,** 3702–3704.
19. Hille, B. (1992) *Ionic Channels in Excitable Membranes* (Sinauer, Sunderland, MA), 2nd Ed.
20. Stühmer, W., Conti, F., Suzuki, H., Wang, X., Noda, M., Yahagi, N., Kubo, H. & Numa, S. (1989) *Nature (London)* **339,** 597–603.
21. Papazian, D. M., Timpe, L. C., Jan, Y. N. & Jan, L. Y. (1989) *Nature (London)* **349,** 305–310.
22. Schoppa, N. E., McCormack, K., Tanouye, M. A. & Sigworth, F. J. (1992) *Science* **255,** 1712–1715.
23. Koeppe, R. E., II, Mazet, J.-L. & Andersen, O. S. (1990) *Biochemistry* **29,** 512–520.